A General Kinematic Model of Fish Locomotion Enables Robot Fish to Master Multiple Swimming Motions

Yong Zhong, *Member, IEEE*, Zicun Hong, *Graduate Student Member, IEEE*,
Yuhan Li, and Junzhi Yu, *Fellow, IEEE*

***Abstract*—Fish locomotion which adopts body and/or caudal fin swimming mode consists of different motions, such as Cruising-straight, Cruising-turn, and various fast turns, etc. Currently, there is no single mathematical model that could illustrate all these motions. Thus, for scientists and engineers, it is quite cumbersome and complicated to model and control different motions with multiple principles. In this paper, we proposed a general kinematic model to illustrate the kinematics of all aforementioned swimming motions. The model is synthesized by a nonlinear oscillator and a traveling wave equation. By changing four parameters extracted from the model, the kinematic model can demonstrate all the aforementioned swimming motions with different amplitudes and frequencies. To verify the model, we built a multi-joint robotic fish, and developed its dynamic model and control method to perform all the maneuvers under the guidance of the general kinematic model. Through this systematic methodology, one can easily study the principles of different swimming motions and design the multi-motions controller for a robotic fish through only one governing kinematic model.**

***Index Terms*—Kinematics, multiple swimming motions, dynamic modeling, robotic fish.**

I. INTRODUCTION

In nature, most fish adopt body and/or caudal fin (BCF) mode to swim, by bending their bodies into a backward-moving propulsive wave to generate thrust [1]. This propulsion method has the advantages of high propulsion efficiency, low noise, and high maneuverability, thus, it has become a research hotspot in the past several decades. A BCF swimmer is very agile and has many different swimming motions. Cruising is the most fundamental swimming behavior observed in fish, which can be classified into two categories: Cruising-straight and Cruising-turn. The former refers to swimming straight at a constant linear speed, while the latter involves swimming with a low angular speed at a constant linear speed [2, 3]. In addition, fast turn motions are also very common. They belong to the unsteady behavior of fish and often appear in the stage of escape or predation. According to the different postures of the fish when turning, it can be divided into C-turn and S-turn, etc, which means the body of the fish will bend into the corresponding shape. [4, 5].

To facilitate scientists and engineers to study the propulsion mode of BCF locomotion, it is necessary to establish its mathematical model. In the elongate-body theory proposed by Lighthill, the traveling wave equation is used to describe the midline body curve of fish [6]. It takes the time and the displacement along the head-tail axis as variables to calculate the lateral displacement of the body. Unlike Lighthill's theory, which takes the lateral displacement of fish body as the control parameter, Petros Koumoutsakos et al. established a mathematical model of the fish body curvature with time and body length, but part of the model is still a cubic spline that needs to be determined by interpolation [7]. These works make it possible to quantitatively analyze the swimming of fish, which greatly broadens the understanding of the effects of fish morphology and flapping parameters.

According to the great advances in turbulence modeling, mesh generation, and linear-system resolution, numerical simulation has become one of the important methods to study the swimming performance of fish. Due to the existence of the traveling wave equation, it is convenient to numerically analyze the locomotion of fish, because the construction of a numerical simulation model can be completed efficiently by changing the individual parameters of the equation [8-10]. However, the traveling wave equation can only be used to illustrate the Cruising-straight motion of fish. The study of other motions of fish is also very attractive, but it is troublesome to perform numerical analysis on them before establishing their kinematic model. Scientists need to take hundreds of photos, and then use interpolation to fit the body curve of fish locomotion [11-13]. If the species or motions of the fish studied change, the work must be repeated. Moreover, it is very difficult to quantitatively

This work was supported in part by the National Natural Science Foundation of China under Grant 62103152, the Natural Science Foundation of Guangdong Province (2022A1515011479), the International cooperation projects of Guangzhou Development Zone (2020GH01), the GuangDong Basic and Applied Basic Research Foundation (No. 2020A1515110584), and the National Key Research and Development Program of China (No. 2017YFB1300200). *(Corresponding author: Yong Zhong).*

Yong Zhong is with Shien-Ming Wu School of Intelligent Engineering, South China University of Technology, Guangzhou, China, and also with Pazhou Lab, Guangzhou, China (email: zhongyong@scut.edu.cn)

Zicun Hong and Yuhan Li are with Shien-Ming Wu School of Intelligent Engineering, South China University of Technology, Guangzhou, China, and also with Pazhou Lab, Guangzhou, China (email: mehong_zicun@mail.scut.edu.cn; 202021058362@mail.scut.edu.cn)

Junzhi Yu is with the State Key Laboratory for Turbulence and Complex Systems, Department of Advanced Manufacturing and Robotics, College of Engineering, Peking University, Beijing (e-mail: junzhi.yu@ia.ac.cn).

analyze the motion model. Therefore, to expand the scope of the application of mathematical model, Petros Koumoutsakos et al. added the baseline curvature to their original model so that the model can describe the motion of the fish's C-turn [14]. In addition, Michel Visonneau et al. also used the curvature of the fish body as a control parameter to establish a mathematical model that can express the switching between the fish swimming forward and turning [15]. Based on these models, a lot of numerical analysis work on the turning performance of fish has been carried out [16, 17]. However, there is no single mathematical model that could illustrate all the aforementioned swimming motions of fish, so the process of numerical analysis of more complex motions is still cumbersome.

With the in-depth study of fish swimming, scientists and engineers began to think about how to combine bionic technology with automation technology, trying to develop robotic fish with better performance than traditional underwater vehicles. In the 1990s, Triantafyllou et al. successfully developed RoboTuna, the first robotic fish in the world [18]. Its emergence has greatly promoted the development of underwater bionic robot technology, including but not limited to structural design, modeling, and control algorithms [19-29]. Our team has also done a lot of work in this field and developed several prototypes of robotic fish [30-33]. In the design of robotic fish, motion control is important, and the trajectory approximation method is a very intuitive and common control method in this field [34]. It makes the robotic fish mimic the locomotion of the real fish by fitting multiple links into the traveling wave curve. However, because the traveling wave equation can only be used to illustrate the Cruising-straight motion of fish, it is complicated to control the robotic fish to perform other motions. For example, when Yu et al. used this method to control the robotic fish, based on the Cruising-straight control model, it is also necessary to apply a specific deflection command to each link of the robotic fish to make it turn in different ways [35-37]. It makes it difficult for researchers to obtain the precise gait of the robotic fish as a whole, which can lead to a decrease in the accuracy of gait control. Many research groups also face the same problem when using this method to control the turning motion of robotic fish [38, 39]. Except for the trajectory approximation method, Central Pattern Generator (CPG) has also been widely used in robotic fish control in recent years [40-42]. CPGs are neural circuits found in many animals that can generate coordinated rhythm signals without high-level command and external feedback input [43, 44]. When researchers use this method to construct a controller, the first task is to establish an appropriate CPG control model. The nonlinear oscillator is a common CPG model in engineering applications. Because it is simple enough to be mathematically tractable, many studies have modified it according to specific needs, to change the time and space characteristics of its output signal. Considering that the body curve of fish can also be regarded as a function related to time and space, we are exploring the possibility of using a nonlinear oscillator to describe its kinematic model, to expand the illustrated range of the kinematic model as much as possible.

In this paper, we propose a general kinematic model that consists of a nonlinear oscillator and a traveling wave equation. It can illustrate the kinematics of Cruising and multiple turning motions of fish by changing the parameters in the model. In addition, a dynamic model of robotic fish is constructed, which can be combined with the proposed general kinematic model to quickly and conveniently analyze the performance of different swimming motions of robotic fish. Finally, a multi-joint robotic fish is built. We carry out numerical simulations on it and design its control algorithm for multiple swimming motions under the guidance of the general kinematic model. The feasibility of the multi-gait control method is verified by experiments and simulations.

The rest of this paper is organized as follows. In Section II, the general kinematic model of fish locomotion is proposed and studied quantitatively. Section III established the dynamics model of the robotics fish base on the general kinematic model. The prototype, numerical simulation analysis, and comparison between experimental and dynamic simulation results are given in Section IV. Finally, Section V contains the conclusion, discussion, and future work.

II. THE GENERAL KINEMATIC MODEL AND QUANTITATIVE ANALYSIS

A. The general kinematic model

Based on the traveling wave equation proposed by Lighthill [6] which describes the midline body curve of fish during Cruising-straight, Alvarado suggested a wave model that counts the "recoil" of the fish [45], and it can be described as:

$$h(x,t) = (c_0 + c_1 x + c_2 x^2) sin(\omega t - kx) \quad (1)$$

where $h(x,t)$ is the lateral displacement of the body, x is the displacement along the head-tail axis, c_0 is the lateral amplitude of the center of geometry of fish swimming, c_1 is the linear wave amplitude envelope, c_2 is the quadratic wave amplitude envelope, k is the body wave number ($k = 2\pi/\lambda$, λ is the body wavelength), and ω is the body wave frequency.

Compared with those equations that use fish body curvature as the control parameter [7, 14, 15], this model is more intuitive and easier to process in application analysis.

In current theories, most body wave models describe the motion state of the fish body from head to tail. However, the heads of many fish swimming in BCF mode are hardly curved and can be regarded as rigid bodies, especially in thunniform motion[1], which means that describing the whole fish body as a traveling wave curve is not quite appropriate. Therefore the general model we proposed below is mainly used to describe the body curve of the force-generating part of the fish body.

In previous work, based on Ijspeert's CPG mode [40], an improved CPG model for controlling wire-driven robotic fish was proposed [41]. The improved model is implemented as a nonlinear oscillator and it can be expressed as:

$$\ddot{b} = k_b(0.25k_b(B - b) - \dot{b}) \quad (2)$$

$$\ddot{m} = k_m(0.25k_m(M - m) - \dot{m}) \quad (3)$$

$$\dot{\phi} = \left[\frac{(1+R)^2}{4R} - \frac{R^2-1}{4R}\text{sign}(\sin\phi)\right]\omega \quad (4)$$

$$\text{sign}(\lambda) = \begin{cases} 1, & \lambda > 0 \\ 0, & \lambda = 0 \\ -1, & \lambda < 0 \end{cases} \quad (5)$$

$$\alpha = b + m\cos(\phi) \quad (6)$$

where b is the offset state, B is the high-level control command of offset, k_b is a positive constant representing how fast b converges to B; m is the amplitude state, M is the high-level control command of amplitude, k_m is a positive constant representing how fast m converges to M; ϕ is the phase state; R is the time ratio between restore phase and beat phase in turning period; ω is the high-level control command of angular velocity (frequency), and the coefficient term of ω is an adjustable step function that can adjust its distribution of different segments within a cycle; α is the oscillation signal output from the CPG model, which is used to control the rotational angle of the servomotor. Based on this CPG model, the fish can achieve smooth adjustment of the oscillation amplitude and smooth switching between Cruising and fast turn motions. It is very informative for the construction of the kinematic model of robotic fish.

Combining the advantages of the traveling wave equation and the CPG model in [41], we propose a general kinematic model to illustrate the kinematics of Cruising-straight, Cruising-turn, and fast turn motion of fish. The model is synthesized by a nonlinear oscillator and a traveling wave:

$$h(x,t) = (c_0 + c_1 x + c_2 x^2)[b(t) + m(t)cos(\phi(t) - kx)] \quad (7)$$

By changing the four parameters B, M, ω, and R, the offset, amplitude, frequency, and time ratio of the kinematic model can be adjusted respectively to mimic the gait of fish. $b(t)$ and $m(t)$ are determined by (2) and (3). They are both second order differential equations, which are critically damped. It means that under this kinematic model, the switching between the different motions of fish is smooth, and the time required for stability after switching can be modulated through k_b and k_m [41]. The larger the k_b and k_m, the shorter the stabilization time. In addition, the adjustable time ratio R of phase makes it very suitable for describing the turning of fish, which usually bends quickly from the initial position to the limit position and restores slowly. The displacement at the end of the curve that the kinematic model describes can be found as:

$$h_{end}(t) = (c_0 + c_1 L + c_2 L^2)[b(t) + m(t)cos(\phi(t) - kL)] \quad (8)$$

where L is the mapping of the fish body length on the head-tail axis.

The max amplitude of the kinematic model is:

$$H = (c_0 + c_1 L + c_2 L^2)(B + M) \quad (9)$$

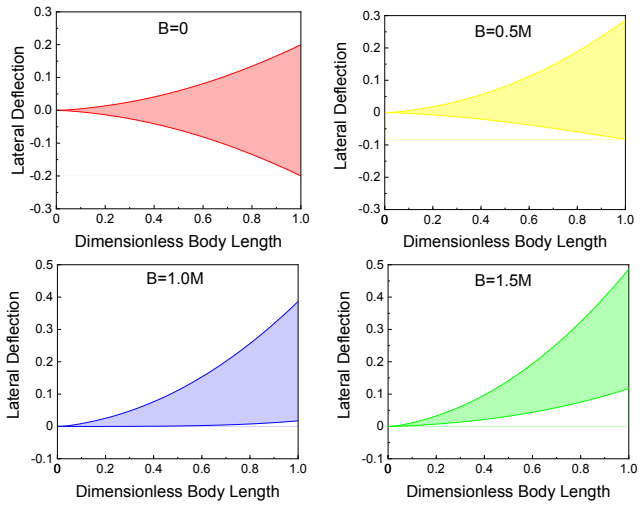

Fig. 1. Swing range of the midline body curve of fish at different B and M.

B. Quantitative analysis of model

To further illustrate the characteristics of this model, we quantitatively analyze its parameters and give the conditions of this model in describing the different motions of fish. Since the traveling wave coefficients (such as c_0, c_1, and c_2) are not the key factors affecting the model's switching to different motions, we choose the appropriate value based on [46].

B and M are commands for offset and amplitude respectively, which control the swing range of the model. We set c_0 = 0, c_1 = 0.05, c_2 = 0.15, k = π/8, M = 1, ω = 2π, R = 1, and change B to analyze its influence on the model. As shown in Fig. 1, when B = 0, the curve oscillates completely symmetrical about the horizontal axis and can be regarded as Cruising-straight motion. When $0 < B < M$, although the oscillation is asymmetric, it is still on both sides of the horizontal axis, and it is consistent with the characteristic of Cruising-turn motion. When $B = M$, the curve is almost parallel to the horizontal axis at the beginning of the beat phase (can also be seen as the end of the restore phase), similar to the posture of fish's C-turn. When $B > M$, the curve is completely tilted to one side of the horizontal axis, which is suitable for describing the maneuver resemble C-turn with smaller angular velocity and turning radius. According to its characteristics, we define it as small radius turn.

In Cruising motion, such as Cruising-straight and Cruising-turn, the oscillation of the fish body is uniform in the time dimension, therefore the time ratio between restore phase and beat phase should be equal to 1 ($R = 1$). We set c_0 = 0, c_1 = 0.05, c_2 = 0.15, k = π, and the control parameters (B, M, ω, R) are set to (0, 1, 2π, 1) to imitate Cruising-straight motion. The simulation results are shown in Fig. 2 (a), which can well reflect the midline body. Recording the change in the displacement at the end of the curve, we can get the influence of M on the model (Fig. 2 (b)). The amplitude of the curve was controlled by M. When M changes from 1 to 2, the amplitude of the curve also doubles. Furthermore, holding the other parameters constant and changing B from 0 to 0.5, the body midline of the Cruising-

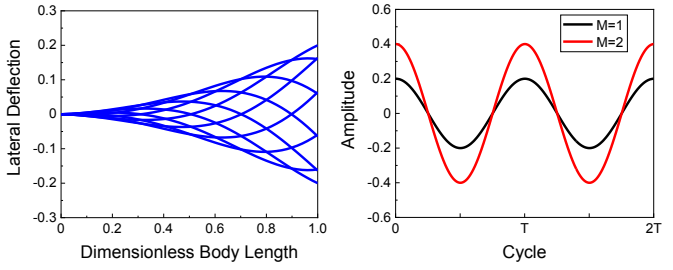

(a) (b)

Fig. 2. Cruising-straight motion of the model. (a) Body curve of Cruising-straight motion. (b) The end of the curve

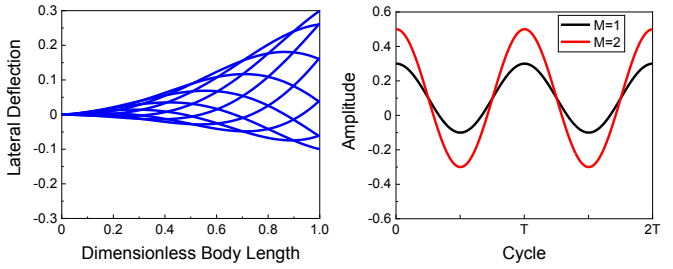

(a) (b)

Fig. 3. Cruising-turn motion of the model. (a) Body curve of Cruising-turn motion. (b) The end of the curve

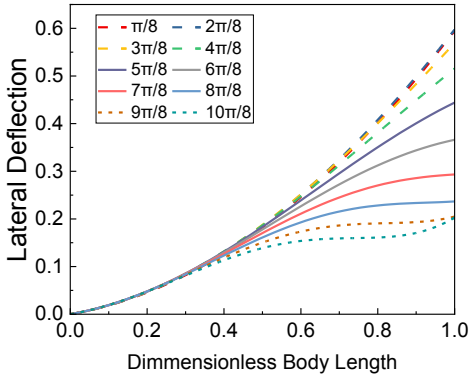

Fig. 4. The influence of k on turning motion

turn can be obtained, as shown in Fig. 3. In summary, it can be concluded that $0 \leq |B| < |M|$, R =1, and $k > 0$ are the conditions for Cruising motion. When $B = 0$, the model represents Cruising-straight, and when $0 < |B| < |M|$, it represents Cruising-turn.

During the turning process, the fish usually bends quickly from the initial position to the limit position and restores slowly. Therefore, when describing turning motion, the time ratio between restore phase and beat phase (t_r/t_b) should be greater than 1, which means $R > 1$ (S-turn is a special case that R is defined as t_b/t_r and it will be explained in the following text).

To determine the influence of the k on the turning motion, we compared the morphology of the kinematic model at different k at the same moment during the beat phase, as shown in Fig. 4. When $k \leq \pi/2$ ($4\pi/8$), the slope of the curve is

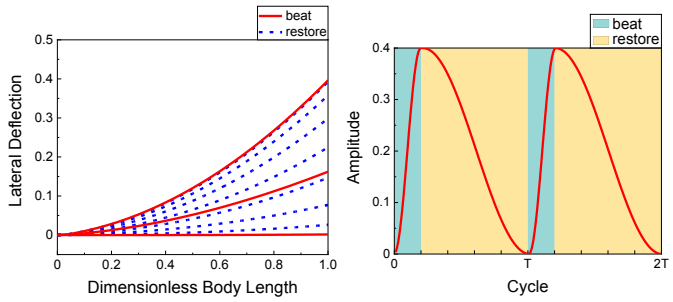

(a) (b)

Fig. 5. C-turn motion of the model($M = 1$, $B = 1$, $k = \pi/32$, $R = 4$). (a) Body curve of C-turn motion. (b) The end of the curve.

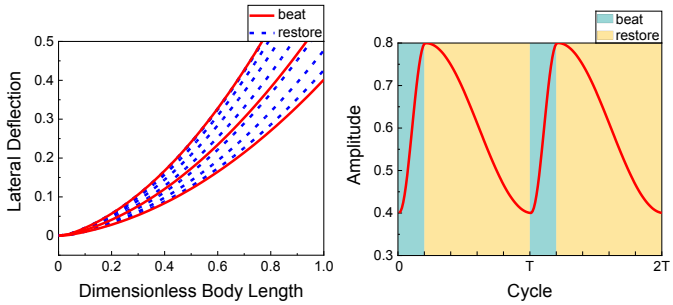

(a) (b)

Fig. 6. Small radius turn motion of the model$(M = 1, B = 3, k = \pi/32, R = 4)$. (a) Body curve of small radius turn motion. (b) The end of the curve.

monotonically increasing with no change in trend, suitable for describing C-turn and Small radius turn. As k continues to increase, the slope of the curve begins to decrease and an inflection point appears. The morphology of the curve at this stage is similar to an S-turn. When $k > \pi$ ($8\pi/8$), the second inflection point appears, and the model no longer belongs to the category of S-turn anymore.

To verify the accuracy of the conditions for different turning motions, by setting $c_0 = 0$, $c_1 = 0.05$, $c_2 = 0.15$, $k = \pi/32$ and $(M, B, \omega, R) = (1, 1, 2\pi, 4)$, we can obtain a fish's C-turn model, as shown in Fig.5 (a). The displacement at the end of the curve in the C-turn motion is shown in Fig. 5(b). We can see that the ratio of restore time (t_r) to beat time (t_b) is 4, which is consistent with $R = t_r/t_b = 4$. It verifies the role of the time ratio R in describing fish turning in our kinematic model. Combined with the quantitative analysis of B, R, and k, we can consider that $|B| = |M|$, $R > 1$, and $0 < k \leq \pi/2$ are the conditions for the model to describe C-turn motion.

Using the same parameter setting as C-turn and adjusting B to 3, we can transform the kinematic model into a form describing fish turning with a small radius, as shown in Fig. 6. Therefore, the conditions for the model to describe the small radius turn motion of fish can be regarded as $|B| > |M|$, $R > 1$, and $0 < k \leq \pi/2$.

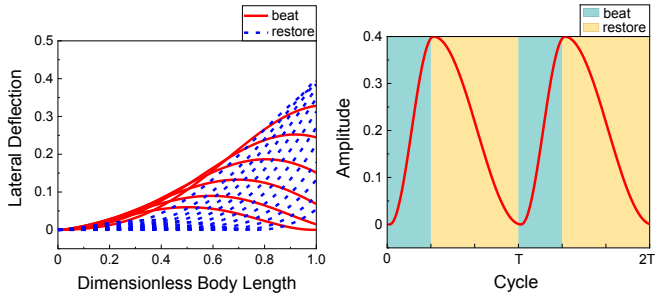

Fig. 7. S-turn motion of the model($M = 1, B = 1, k = \pi, R = 0.5$). (a) Body curve S-turn motion. (b) The end of the curve.

TABLE I
CONDITIONS TO DESCRIBE VARIOUS MOTIONS OF THE MODEL

Motion	B	R	k
Cruising-straight	$B = 0$	$R = 1$	$k > 0$
Cruising-turn	$0 < \|B\| < \|M\|$	$R = 1$	$k > 0$
C-turn	$\|B\| = \|M\|$	$R > 1$	$0 < k \leq \pi/2$
Small radius turn	$\|B\| > \|M\|$	$R > 1$	$0 < k \leq \pi/2$
S-turn	$\|B\| \geq \|M\|$	$R < 1$	$\pi/2 < k \leq \pi$

The quantitative analysis of k (Fig. 4) shows that $\pi/2 < k \leq \pi$ is suitable for the model to describe the fish's S-turn. It should be noted that because S-turn has two peaks with different trends, the tendency of the displacement of its end is opposite to that of the C-turn with only one peak. It means that R is equal to the time ratio of beat phase to restore phase ($R = t_b/t_r$), which should be less than 1. By setting $c_0 = 0$, $c_1 = 0.05$, $c_2 = 0.15$, $k = \pi$ and $(M, B, \omega, R) = (1, 1, 2\pi, 0.5)$, we can obtain a fish's S-turn model, as shown Fig. 7. It's conditions are $|B| \geq |M|$, $R < 1$, and $\pi/2 < k \leq \pi$.

A series of analyses have indicated that each parameter in the model has a corresponding impact on the morphology of the curve. After the summary, the conditions to describe various motions of the model are shown in Table I.

III. THE DYNAMICS OF ROBOTIC FISH BASED ON THE GENERAL MODEL

A. The dynamics of robotic fish

The dynamic modeling methods of multi-articulated robots have been extensively studied [47-49]. In recent years, Pettersen et al. [50, 51] have done a lot of work on underwater snake robots. Their modeling approach considers hydrostatic forces, hydrodynamic, and torques, and avoids the numerical evaluation of drag effects. As the object of their study is a snake robot, the dimensions of each joint are treated as the same to simplify modeling. However, for robotic fish, the differences between the joints are more pronounced, such as a wide head and a thin tail. It means that uniformized modeling

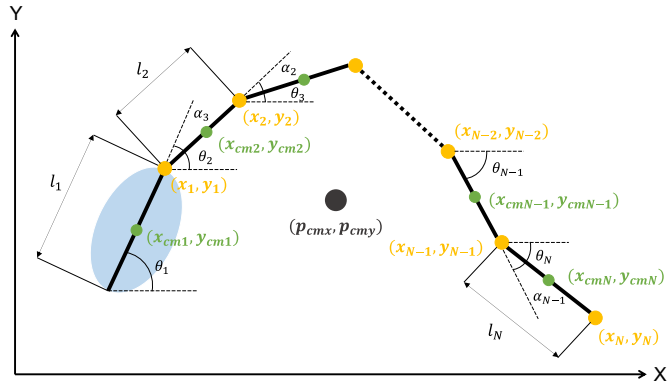

Fig. 8. The simplified model of robotic fish

of joints may produce large errors. Therefore, we have made a few modifications to the model so that the dimensions of each joint can be set individually to meet the shape of the robotic fish.

When analyzing the dynamics of robotic fish, we regard its body model as consisting of N rigid links, which means it has a total of $N-1$ rotational joints. The center of mass (CM) of each link is located at the center point. The simplified model is shown in Fig. 8.

We simplify each link into an elliptic cylinder, and use vector $\mathbf{a}$, $\mathbf{b}$, $\mathbf{l}$, $\mathbf{m}$ and $\mathbf{J}$ to represent the major radius, minor radius, length, mass and moment of inertia of links respectively. They can be expressed as

$$\mathbf{a} = \mathrm{diag}[a_1, \dots, a_N] \in \mathbb{R}^{N\times N} \tag{10}$$

$$\mathbf{b} = \mathrm{diag}[b_1, \dots, b_N] \in \mathbb{R}^{N\times N} \tag{11}$$

$$\mathbf{l} = \mathrm{diag}[l_1, \dots, l_N] \in \mathbb{R}^{N\times N} \tag{12}$$

$$\mathbf{m} = \mathrm{diag}[m_1, \dots, m_N] \in \mathbb{R}^{N\times N} \tag{13}$$

$$\mathbf{J} = \frac{1}{3}\mathrm{diag}[m_1 l_1, \dots, m_N l_N] \in \mathbb{R}^{N\times N} \tag{14}$$

For the sake of calculation, we will use the following notation when modeling the dynamics of the robotic fish.

$$\mathbf{A} = \begin{bmatrix} 1 & 1 & & \\ & \ddots & \ddots & \\ & & 1 & 1 \end{bmatrix}, \mathbf{D} = \begin{bmatrix} 1 & -1 & & \\ & \ddots & \ddots & \\ & & 1 & -1 \end{bmatrix} \tag{15}$$

Where $\mathbf{A}, \mathbf{D} \in \mathbb{R}^{(N-1)\times N}$.

$$\mathbf{e} = [1, \quad \dots, \quad 1]^T \in \mathbb{R}^N, \ \mathbf{E} = \begin{bmatrix} \mathbf{e} & \mathbf{0}_{N\times 1} \\ \mathbf{0}_{N\times 1} & \mathbf{e} \end{bmatrix} \in \mathbb{R}^{2N\times 2} \tag{16}$$

$$\sin\boldsymbol{\theta} = [\sin\theta_1, \quad \dots, \quad \sin\theta_N]^T \in \mathbb{R}^N \tag{17}$$

$$\mathbf{S}_\theta = \mathrm{diag}(\sin\boldsymbol{\theta})\mathbb{R}^{N\times N} \tag{18}$$

$$\cos\boldsymbol{\theta} = [\cos\theta_1, \quad \dots, \quad \cos\theta_N]^T \in \mathbb{R}^N \tag{19}$$

$$\mathbf{C}_\theta = \mathrm{diag}(\cos\boldsymbol{\theta})\mathbb{R}^{N\times N} \tag{20}$$

The notations **A** and **D** represent "addition" and "difference" in matrix operation, and the notation **e** is used for the summation of vectors.

We use vectors $\boldsymbol{\theta} = [\theta_1, \ldots, \theta_{\mathrm{N}}]^T \in \mathrm{R}^N$ and $\boldsymbol{\alpha} = [\alpha_1, \ldots, \alpha_{\mathrm{N}-1}]^T \in \mathbb{R}^{N-1}$ to represent the aggregate of the link angle and joint angle respectively.

The position of the CM(center of mass) of the robotic fish is

$$\mathbf{P}_{\mathrm{CM}} = \begin{bmatrix} P_{\mathrm{cmx}} \\ P_{\mathrm{cmy}} \end{bmatrix} = \begin{bmatrix} \frac{1}{M}\sum_{i=1}^{N} m_i x_{\mathrm{cmi}} \\ \frac{1}{M}\sum_{i=1}^{N} m_i y_{\mathrm{cmi}} \end{bmatrix} = \frac{1}{\mathrm{M}} \begin{bmatrix} \mathbf{m}\mathbf{X}_{\mathrm{cm}} \\ \mathbf{m}\mathbf{Y}_{\mathrm{cm}} \end{bmatrix} \quad (21)$$

where M is the total mass of the robotic fish, (x_{cmi}, y_{cmi}) are the coordinate of the CM of link i, $\mathbf{X}_{\mathrm{cm}} = [x_{\mathrm{cm1}}, \ldots, x_{\mathrm{cmN}}]^{\mathrm{T}} \in \mathbb{R}^{\mathrm{N}}$ and $\mathbf{Y}_{\mathrm{cm}} = [y_{\mathrm{cm1}}, \ldots, y_{\mathrm{cmN}}]^{\mathrm{T}} \in \mathbb{R}^{\mathrm{N}}$.

Based on the constraints of the adjacent links i and $i+1$, we can get all links' joint constraints of the robotic fish:

$$\begin{cases} \mathbf{D}\mathbf{X}_{\mathrm{cm}} + \mathbf{A}\left(\frac{\mathrm{l}}{2}\cos\boldsymbol{\theta}\right) = 0 \\ \mathbf{D}\mathbf{Y}_{\mathrm{cm}} + \mathbf{A}\left(\frac{\mathrm{l}}{2}\sin\boldsymbol{\theta}\right) = 0 \end{cases} \quad (22)$$

To solve the position of the individual links, we combine (21) and (22) into

$$\mathbf{T}\mathbf{X}_{\mathrm{cm}} = \begin{bmatrix} -\mathbf{A}\left(\frac{\mathrm{l}}{2}\cos\boldsymbol{\theta}\right) \\ P_{\mathrm{cmx}} \end{bmatrix}, \quad \mathbf{T}\mathbf{Y}_{\mathrm{cm}} = \begin{bmatrix} -\mathbf{A}\left(\frac{\mathrm{l}}{2}\sin\boldsymbol{\theta}\right) \\ P_{\mathrm{cmy}} \end{bmatrix} \quad (23)$$

$$\mathbf{T} = \begin{bmatrix} \mathbf{D} \\ \frac{1}{\mathrm{M}}\mathbf{m} \end{bmatrix} \in \mathbb{R}^{N \times N} \quad (24)$$

where **T** is nonsingular and thereby invertible, so we can express the position of the individual links with CM position and link angles of robotic fish:

$$\mathbf{X}_{\mathrm{cm}} = \mathbf{T}^{-1} \begin{bmatrix} -\mathbf{A}\left(\frac{\mathrm{l}}{2}\cos\boldsymbol{\theta}\right) \\ P_{\mathrm{cmx}} \end{bmatrix} \in \mathbb{R}^{N \times 1} \quad (25)$$

$$\mathbf{Y}_{\mathrm{cm}} = \mathbf{T}^{-1} \begin{bmatrix} -\mathbf{A}\left(\frac{\mathrm{l}}{2}\sin\boldsymbol{\theta}\right) \\ P_{\mathrm{cmy}} \end{bmatrix} \in \mathbb{R}^{N \times 1} \quad (26)$$

By differentiating the position of individual links with respect to time, we can obtain its velocity

$$\dot{\mathbf{X}}_{\mathrm{cm}} = \mathbf{T}^{-1} \begin{bmatrix} \mathbf{A}\left(\mathbf{S}_\theta \dot{\boldsymbol{\theta}}\right) \\ \dot{P}_{\mathrm{cmx}} \end{bmatrix} \in \mathbb{R}^{N \times 1} \quad (27)$$

$$\dot{\mathbf{Y}}_{\mathrm{cm}} = \mathbf{T}^{-1} \begin{bmatrix} -\mathbf{A}\left(\mathbf{C}_\theta \dot{\boldsymbol{\theta}}\right) \\ \dot{P}_{\mathrm{cmy}} \end{bmatrix} \in \mathbb{R}^{N \times 1} \quad (28)$$

Further, by differentiating the velocity, the acceleration of individual links can be obtained

$$\ddot{\mathbf{X}}_{\mathrm{cm}} = \mathbf{T}^{-1} \begin{bmatrix} \mathbf{A}\left(\frac{\mathrm{l}}{2}\mathbf{C}_\theta \dot{\boldsymbol{\theta}}^2 + \frac{\mathrm{l}}{2}\mathbf{S}_\theta \ddot{\boldsymbol{\theta}}\right) \\ \ddot{P}_{\mathrm{cmx}} \end{bmatrix} \in \mathbb{R}^{N \times 1} \quad (29)$$

$$\ddot{\mathbf{Y}}_{\mathrm{cm}} = \mathbf{T}^{-1} \begin{bmatrix} \mathbf{A}\left(\frac{\mathrm{l}}{2}\mathbf{S}_\theta \dot{\boldsymbol{\theta}}^2 - \frac{\mathrm{l}}{2}\mathbf{C}_\theta \ddot{\boldsymbol{\theta}}\right) \\ \ddot{P}_{\mathrm{cmy}} \end{bmatrix} \in \mathbb{R}^{N \times 1} \quad (30)$$

When the robotic fish swim in the water, the force balance equation of all links can be expressed as

$$\mathbf{m}\ddot{\mathbf{X}}_{\mathrm{cm}} = \mathbf{D}^{\mathbf{T}}\mathbf{h}_{\mathbf{x}} + \mathbf{f}_{\mathbf{x}}, \quad \mathbf{m}\ddot{\mathbf{Y}}_{\mathrm{cm}} = \mathbf{D}^{\mathbf{T}}\mathbf{h}_{\boldsymbol{y}} + \mathbf{f}_{\mathbf{y}} \quad (31)$$

where vector $\mathbf{h}=[h_x, h_y]^{\mathrm{T}} \in \mathbb{R}^{\mathrm{N-1}}$ and $\mathbf{f} = [f_x, f_y]^{\mathrm{T}} \in \mathbb{R}^{\mathrm{N}}$ are the joint constraint forces and fluid forces acting on links, respectively. The joint constraint force on links in the direction of the x and y axes in the global coordinate system are $\mathbf{h_x} = [h_1, \cdots, h_{\mathrm{N}-1}]^{\mathrm{T}} \in \mathbb{R}^{\mathrm{N}-1}$ and $\mathbf{h_y} = [h_1, \cdots, h_{\mathrm{N}-1}]^{\mathrm{T}} \in \mathbb{R}^{\mathrm{N}-1}$, respectively.

In the mechanical analysis of the robotic fish as a whole, the joint constraint forces cancel each other, so we can get the acceleration of the CM of the robotic fish

$$\begin{bmatrix} \ddot{P}_{\mathrm{cmx}} \\ \ddot{P}_{\mathrm{cmy}} \end{bmatrix} = \frac{1}{\mathrm{M}} \begin{bmatrix} \mathbf{e}^{\mathbf{T}} & \mathbf{0} \\ \mathbf{0} & \mathbf{e}^{\mathbf{T}} \end{bmatrix} \begin{bmatrix} \mathbf{f}_{\mathrm{x}} \\ \mathbf{f}_{y} \end{bmatrix} \quad (32)$$

The torque balance equation of all links is given by

$$\mathbf{J}\ddot{\boldsymbol{\theta}} = \mathbf{D}^{\mathrm{T}}\mathbf{t} - \mathbf{l}\mathbf{S}_\theta \mathbf{A}^{\mathrm{T}}\mathbf{h}_{\mathbf{x}} + \mathbf{l}\mathbf{C}_\theta \mathbf{A}^{\mathrm{T}}\mathbf{h}_{\mathbf{y}} + \boldsymbol{\tau} \quad (33)$$

where vector $\mathbf{t} = [t_1, \cdots, t_{\mathrm{N}}]^{\mathrm{T}} \in \mathbb{R}^{\mathrm{N}-1}$ represents the actuator torque of the joint. According to combine (31) into (32), we can replace $\mathbf{h_x}$ and $\mathbf{h_y}$ with $\ddot{\mathbf{X}}_{\mathrm{cm}}$ and **f**.

The fluid torque acting on all links can be expressed as

$$\boldsymbol{\tau} = -\boldsymbol{\lambda_1}\ddot{\boldsymbol{\theta}} - \boldsymbol{\lambda_2}\dot{\boldsymbol{\theta}} - \boldsymbol{\lambda_3}\mathrm{diag}\left(\mathrm{sgn}(\dot{\boldsymbol{\theta}})\right)\dot{\boldsymbol{\theta}}^{\mathbf{2}} \quad (34)$$

where vector $\boldsymbol{\lambda_1}, \boldsymbol{\lambda_2}, \boldsymbol{\lambda_3}$ depend on the fluid characteristics and the shape of each joint of robotic fish [50]. For the elliptic cylinder, we have

$$\begin{aligned} \boldsymbol{\lambda_1} &= \frac{\mathbf{1}}{\mathbf{96}}\mathrm{C_M}(\mathbf{a}^2 + \mathbf{b}^2)\mathbf{l}^3 \in \mathbb{R}^{N \times N} \\ \boldsymbol{\lambda_2} &= \frac{\mathbf{1}}{\mathbf{48}}\rho\pi\mathrm{C_f}(\mathbf{a} + \mathbf{b})\mathbf{l}^3 \in \mathbb{R}^{N \times N} \\ \boldsymbol{\lambda_3} &= \frac{\mathbf{1}}{\mathbf{128}}\rho\pi\mathrm{C_f}(\mathbf{a} + \mathbf{b})\mathbf{l}^4 \in \mathbb{R}^{N \times N} \end{aligned} \quad (35)$$

where $\mathrm{C_M}$ is the added inertia coefficient, $\mathrm{C_f}$ is the drag coefficient, and ρ is the density of the fluid.

When calculating the hydrodynamic force, we need to transform the relative velocity between the links and the water from the global frame coordinate into the body frame coordinate, and the transformation matrix is

$$\mathbf{R}_{\mathrm{link,i}}^{\mathrm{global}} = \begin{bmatrix} \cos\theta_i & -\sin\theta_i \\ \sin\theta_i & \cos\theta_i \end{bmatrix} \quad (36)$$

Therefore, the relative velocity between the links and the water in body frame coordinates are

$$\begin{bmatrix}\mathbf{V_{rx}}\\ \mathbf{V_{ry}}\end{bmatrix}=\begin{bmatrix}\mathbf{C}_\theta & \mathbf{S}_\theta\\ -\mathbf{S}_\theta & \mathbf{C}_\theta\end{bmatrix}\begin{bmatrix}\dot{\mathbf{X}}_{\mathrm{cm}}-\mathbf{V_x}\\ \dot{\mathbf{Y}}_{\mathrm{cm}}-\mathbf{V_y}\end{bmatrix} \tag{37}$$

where the vector $\mathbf{V_x}\in\mathbb{R}^{N\times1}$ and $\mathbf{V_y}\in\mathbb{R}^{N\times1}$ are the components of the flow velocity in the x and y directions in the global coordinate respectively (assume flow velocity is constant and irrotational).

Furthermore, we can get the relative acceleration of the links

$$\begin{bmatrix}\dot{\mathbf{V}}_{\mathbf{rx}}\\ \dot{\mathbf{V}}_{\mathbf{ry}}\end{bmatrix}=\begin{bmatrix}\mathbf{C}_\theta & \mathbf{S}_\theta\\ -\mathbf{S}_\theta & \mathbf{C}_\theta\end{bmatrix}\begin{bmatrix}\ddot{\mathbf{X}}_{\mathrm{cm}}\\ \ddot{\mathbf{Y}}_{\mathrm{cm}}\end{bmatrix}+\begin{bmatrix}-\mathbf{S}_\theta & \mathbf{C}_\theta\\ -\mathbf{C}_\theta & -\mathbf{S}_\theta\end{bmatrix}\begin{bmatrix}\mathrm{diag}(\dot{\boldsymbol{\theta}}) & \mathbf{0}\\ \mathbf{0} & \mathrm{diag}(\dot{\boldsymbol{\theta}})\end{bmatrix}\begin{bmatrix}\dot{\mathbf{X}}_{\mathrm{cm}}-\mathbf{V_x}\\ \dot{\mathbf{Y}}_{\mathrm{cm}}-\mathbf{V_y}\end{bmatrix} \tag{38}$$

The fluent forces exerted on the links can be expressed as

$$\mathbf{f}=\begin{bmatrix}\mathbf{f_x}\\ \mathbf{f_y}\end{bmatrix}=\begin{bmatrix}\mathbf{f_{A_x}}\\ \mathbf{f_{A_y}}\end{bmatrix}+\begin{bmatrix}\mathbf{f}^{\mathrm{I}}_{\mathbf{D_x}}\\ \mathbf{f}^{\mathrm{I}}_{\mathbf{D_y}}\end{bmatrix}+\begin{bmatrix}\mathbf{f}^{\mathrm{II}}_{\mathbf{D_x}}\\ \mathbf{f}^{\mathrm{II}}_{\mathbf{D_y}}\end{bmatrix} \tag{39}$$

where the vectors $\mathbf{f_{A_x}}$ and $\mathbf{f_{A_y}}$ represent the added mass effects and they are given by

$$\begin{bmatrix}\mathbf{f_{A_x}}\\ \mathbf{f_{A_y}}\end{bmatrix}=\begin{bmatrix}\mathbf{C}_\theta & -\mathbf{S}_\theta\\ \mathbf{S}_\theta & \mathbf{C}_\theta\end{bmatrix}\begin{bmatrix}\boldsymbol{\mu_t} & \mathbf{0}\\ \mathbf{0} & \boldsymbol{\mu_n}\end{bmatrix}\begin{bmatrix}\dot{\mathbf{V}}_{\mathbf{rx}}\\ \dot{\mathbf{V}}_{\mathbf{ry}}\end{bmatrix} \tag{40}$$

where $\boldsymbol{\mu_n}=\rho\pi C_A\mathbf{a}^2\mathbf{l}$, C_A is the added mass coefficient in the normal direction. The added mass effects of a slender body in tangential direction can be neglected, so $\boldsymbol{\mu_t}=0$.

The vectors $\mathbf{f_{D_x}}$ and $\mathbf{f_{D_y}}$ represent the drag forces. They divide into linear drag forces $\mathbf{f}^{\mathrm{I}}_{\mathbf{D_x}}, \mathbf{f}^{\mathrm{I}}_{\mathbf{D_y}}$ and nonlinear drag forces $\mathbf{f}^{\mathrm{II}}_{\mathbf{D_x}}, \mathbf{f}^{\mathrm{II}}_{\mathbf{D_Y}}$

$$\begin{bmatrix}\mathbf{f}^{\mathrm{I}}_{\mathbf{D_x}}\\ \mathbf{f}^{\mathrm{I}}_{\mathbf{D_y}}\end{bmatrix}=-\begin{bmatrix}\mathbf{c_t}\mathbf{C}_\theta & -\mathbf{c_n}\mathbf{S}_\theta\\ \mathbf{c_t}\mathbf{S}_\theta & \mathbf{c_n}\mathbf{C}_\theta\end{bmatrix}\begin{bmatrix}\mathbf{V_{rx}}\\ \mathbf{V_{ry}}\end{bmatrix} \tag{41}$$

$$\begin{bmatrix}\mathbf{f}^{\mathrm{II}}_{\mathbf{D_x}}\\ \mathbf{f}^{\mathrm{II}}_{\mathbf{D_y}}\end{bmatrix}=-\begin{bmatrix}\mathbf{c_t}\mathbf{C}_\theta & -\mathbf{c_n}\mathbf{S}_\theta\\ \mathbf{c_t}\mathbf{S}_\theta & \mathbf{c_n}\mathbf{C}_\theta\end{bmatrix}\mathrm{diag}\left(\mathrm{sgn}\left(\begin{bmatrix}\mathbf{V_{rx}}\\ \mathbf{V_{ry}}\end{bmatrix}\right)\right)\begin{bmatrix}\mathbf{V_{rx}}^2\\ \mathbf{V_{ry}}^2\end{bmatrix} \tag{42}$$

where $\mathbf{c_t}=\frac{1}{2}\rho\pi C_f\frac{(\mathbf{b}+\mathbf{a})}{2}\mathbf{l}\in\mathbb{R}^{\mathrm{N}}$, $\mathbf{c_n}=\frac{1}{2}\rho C_D 2\mathbf{a}\mathbf{l}\in\mathbb{R}^{\mathrm{N}}$, C_f and C_D are the drag coefficients in tangential and normal direction of the links.

The construction of the robotic fish dynamic model can help us intuitively analyze the swimming performance of robotic fish under different gait. The dynamic simulation results will be displayed together with the experimental results in Section IV.

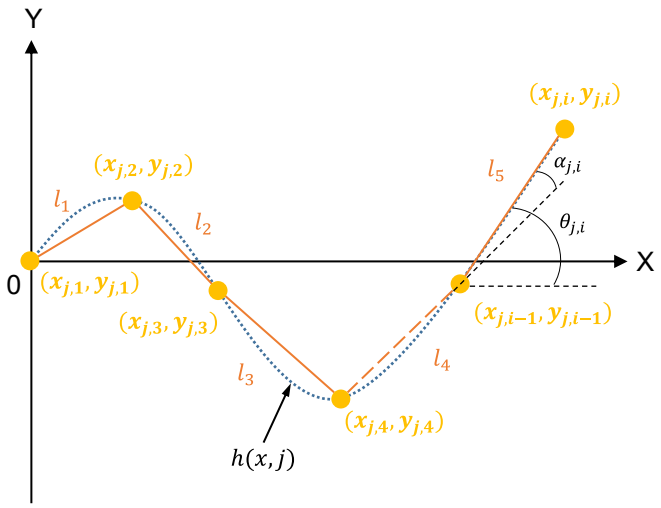

Fig. 9. Curve fitting based on the general kinematic model

B. Joint input based on the general model

To transform the general model into joint input, we need to discretize the general model in the time dimension:

$$h(x,j)=(c_0+c_1x+c_2x^2)\left[b(\tfrac{Tj}{\mathrm{U}})+m(\tfrac{Tj}{\mathrm{U}})cos\left(\phi\left(\tfrac{Tj}{\mathrm{U}}\right)-kx\right)\right]\quad j=1,\dots,\mathrm{U}. \tag{43}$$

where T is the time of a cycle, U is the number that the whole cycle is divided into, representing the discrete degree of the control model in time, and j denotes the jth time oscillating sequence of the model.

As shown in Fig. 8, the coordinate of each joint of the robotic fish is (x_i, y_i). To calculate the rotation angle of each joint of the robotic fish based on the general model, regard the tail end as one of the joints. Combining the geometric constraints of the robotic fish with equation (43), we can calculate the position of each link in the moving chain by numerical fitting, as shown in Fig 9. The coordinates of the robotic fish's joint should meet the following conditions:

$$\begin{aligned}&(x_{j,i}-x_{j,i-1})^2+(y_{j,i}-y_{j,i-1})^2=l_i^2\\ &y_{j,i}=(c_0+c_1x_{j,i}+c_2{x_{j,i}}^2)\left[b(\tfrac{Tj}{\mathrm{U}})+m(\tfrac{Tj}{\mathrm{U}})cos\left(\phi\left(\tfrac{Tj}{\mathrm{U}}\right)-kx_{j,i}\right)\right]\\ &j=1,\dots,\mathrm{U};\ \ i=2,\dots,\mathrm{N}.\end{aligned} \tag{44}$$

where i indicates the ith link, j denotes the jth oscillating sequence, and N is the number of links.

Because the general model describes the kinematics of the part of the fish producing forces (excluding it's rigid head), we let the head of the robotic fish parallel to the x-axis which means $\theta_1=0$, and set the initial joint coordinate $(x_{j,1}, y_{j,1})$ to (0, 0). After a series of iterative operations, we can get the other joint

coordinates $(x_{j,i}, y_{j,i})$. Therefore, under the jth oscillation sequence, the angle between the *i*th link and *x*-axis is:

$$\theta_{j,i} = \arctan\frac{y_{j,i}-y_{j,i-1}}{x_{j,i}-x_{j,i-1}} \quad j = 1, \dots, \mathrm{U}; \quad i = 2, \dots, \mathrm{N}. \quad (45)$$

the rotation angle of each joint can be defined as:

$$\alpha_{j,i} = \theta_{j,i} - \theta_{j,i-1} \quad j = 1, \dots, \mathrm{U}; \quad i = 2, \dots, \mathrm{N}. \quad (46)$$

Depending on the data set of each joint angle in each frame, the multiple motions' accurate control of the robotic fish can be realized. In the simulation of the dynamics model of the robotic fish, the target angle of the joint needs to be converted into the required input torque **t**. This process can be completed through the PD controller. By Substituting the torque **t** into equation(33) and combining equation (29) (30) (31) for iterative calculation, the robotic fish dynamics based on the general model can be obtained.

When calculating the input torque of each joint, the selected PD controller can be expressed as

$$u_i = K_{p,i}(\alpha_i^* - \alpha_i) - K_{d,i}\dot{\alpha}_i \quad i = 1, \dots, \mathrm{N}-1. \quad (47)$$

where $K_{p,i}$ and $K_{d,i}$ are the gains of the controller, α_i^* is the target angle of each joint, α_i is the current angle of each joint.

IV. Simulations and Experiments

A. Multi-joint robotic fish system

The general kinematic model can provide guidance for the design of the motion control algorithm. We built a multi-joint robotic fish as an experimental prototype to verify the control effect, as shown in Fig. 10. The robotic fish has five driving joints, and its tail at the end can be quickly replaced to imitate the swimming characteristics of different types of fish. Its control board and power supply are external to the body, and the transmission of control signals is completed through cables. The design details of the robotic fish platform have been introduced in [52].

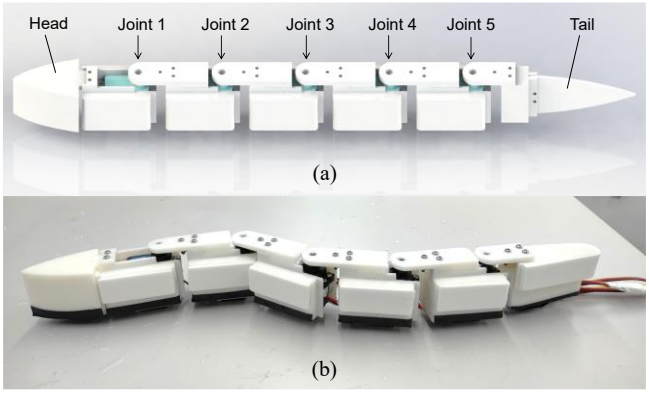

Fig. 10. Multi-joint robotic fish. (a) the CAD model. (b) the prototype.

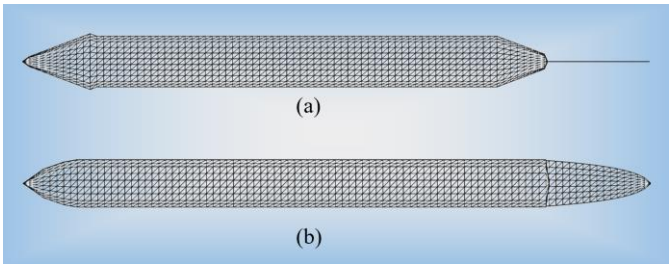

Fig. 11. The CFD model. (a) top view. (b) side view.

B. Numerical simulation

Before the prototype experiment, the numerical simulation can not only provide a reference for the control algorithm, but also help us to analyze the swimming performance of the robotic fish under different motions in detail. According to the overall dimensions of the multi-joint robotic fish, we built its CFD model, as shown in Fig. 11. In this paper, we use the finite difference–immersed boundary method to solve the dynamics of the fluid around the swimmer. The governing equations for the fluid around the swimmer are as follows:

$$\nabla \cdot \mathbf{u} = 0 \quad (48)$$

$$\frac{\partial \mathbf{u}}{\partial \mathbf{t}} + (\mathbf{u} \cdot \nabla)\mathbf{u} = -\frac{1}{\rho}\nabla p + v\Delta\mathbf{u} \quad (49)$$

where **u** denotes the velocity vector, p denotes the pressure, and ρ and v are the density and viscosity of water, respectively. The fluid solver is able to simulate the motion of complex embedded objects, including zero-thickness membranes and three-dimensional solids, and has been successfully applied to the swimming of fish [53, 54].

Since there is no kinematic model that can describe multiple motions of fish before, each motion (such as Cruising or fast turn) should be analyzed separately in the numerical simulation. As a result, multiple kinematic models need to be applied in the analysis of different motions, which causes the process more complicated, and it is impossible to study the switching process of different motions. Based on the general kinematic model proposed in this paper, we can set the step function to modify the parameters in the model during simulation, which can realize the smooth switching of different motions and greatly expand the range of numerical analysis.

We choose the Cruising-straight to S-turn as an example to verify the effect of CFD applied to different motion switching. In Cruising-straight motion, $M = 3$, $B = 0$, $R = 1$, $k = \pi$, $\omega = 2\pi$. At the fourth second of the simulation, change B to 3 and R to 0.7, then the motion will start to switch to S-turn. The k_b can control the switching speed from b to B. It can be seen from Fig.12 that when k_b is equal to 5, 10, 15, the time for b to converge to B is 3.16s, 1.58s, 1.05s respectively. The larger the k_b, the faster the switch will be. The smooth switching of the kinematics model between different motions can prevent errors caused by parameter mutation during numerical simulation. In

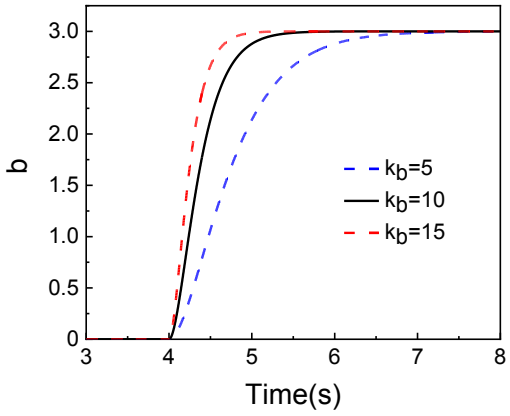

Fig. 12. Convergence of b at different k_b.

this numerical simulation, we set k_b to 10. Fig. 13 shows the simulation process of robotic fish switching between different motions. The color of the area where the fish swims through indicates the velocity of the vortex, expressed in Body Length/Period (BL/T). The moment refers to the rotational effect of hydrodynamic forces on robotic fish. As shown in Fig. 14, it is clear that the change of the moment before 4s is symmetrical about 0, but after that, the positive peak of the moment is significantly greater than the negative peak (the positive/negative moment corresponds to the clockwise-/counterclockwise motion of the robotic fish respectively). By integrating the moment with time, the angular impulse obtained in each swimming cycle of the robotic fish can be calculated (which reflected the rotation trend of the robotic fish in each cycle), and the result is shown in Fig. 15.

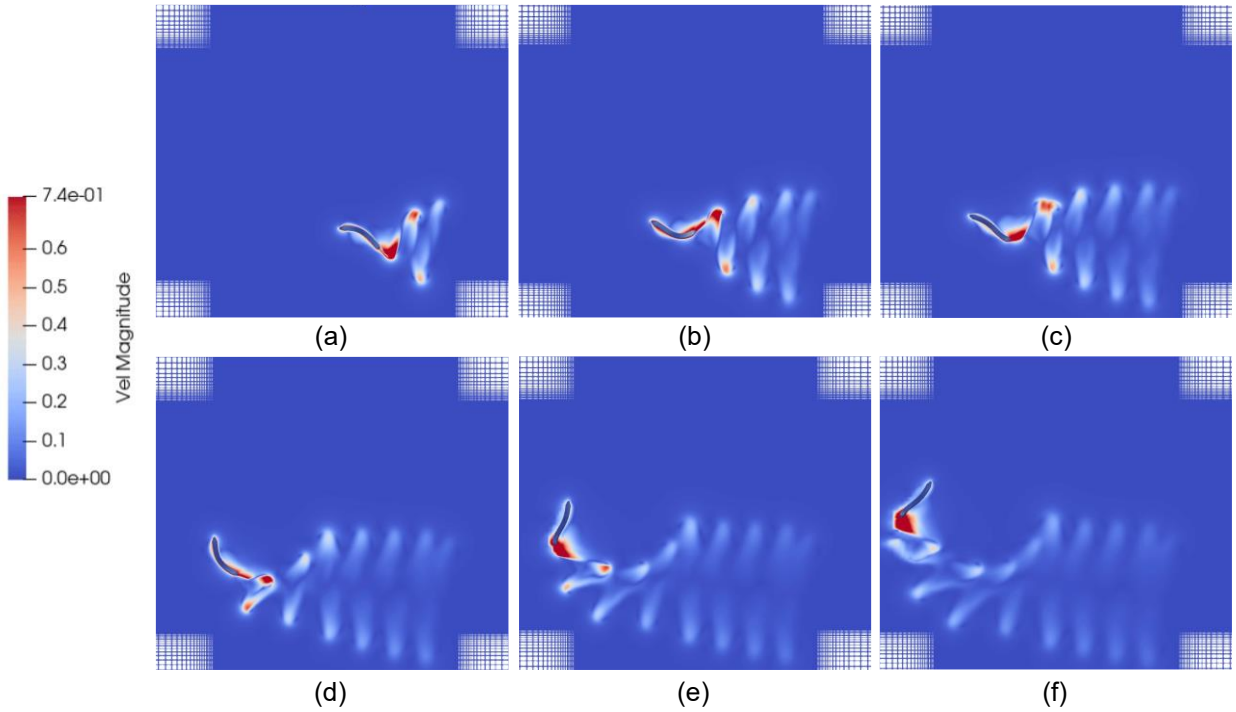

Fig. 13. Snapshot sequence of the CFD simulation of robotic fish switching from Cruising-straight to S-turn. (a) 1.5s. (b) 3s. (c) 4.5s. (d) 6s. (e) 7.5s. (f) 9s.

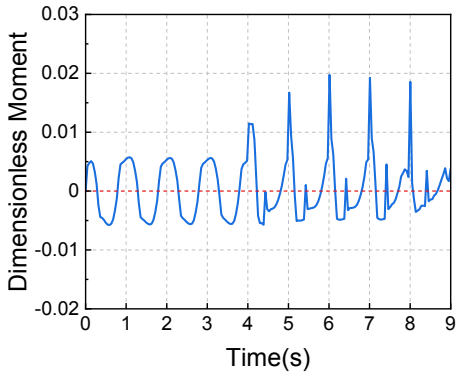

Fig. 14. Moment of force on the robotic fish as it swims.

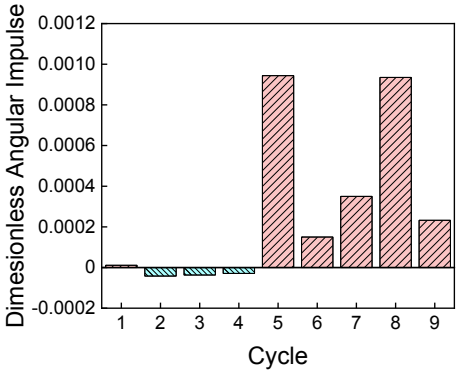

Fig. 15. Angular impulse on the robotic fish in each swimming cycle.

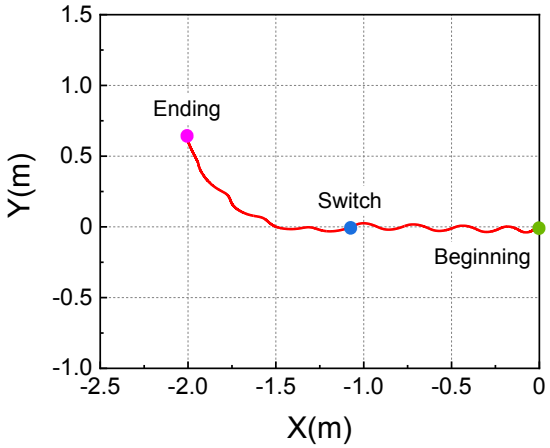

Fig. 16. The trajectory of robotic fish in the numerical simulation.

It can be seen that in the first four cycles, the angular impulse is essentially equal to 0. However, from the 5th cycle onwards, all angular impulse are positive and of a much larger magnitude than the first four cycles, which will induce the robotic fish to turn clockwise. Fig. 16 records the trajectory of robotic fish in the CFD simulation. It illustrates that the robotic fish successfully switched from Cruising-straight to S-turn in the fourth second.

C. Stationary tests

In the experiment to test whether the algorithm can accurately control the body posture of the robotic fish, the head of the robotic fish is fixed, which is convenient for us to observe the change in its body posture. We combine equations (43)~(46), discretize each motion cycle of the robotic fish into 20 frames (U = 20), and adjust the parameters of the general kinematic model to make the robotic fish swing according to different swimming motions. It should be noted that all joints are used to fit the general kinematic model to make the distinction between the postures of each motion greater (different from free swimming tests). c_0, c_1, and c_2 of the kinematic model are set to 0, 0.05 and 0.15. The settings of the rest parameters are shown in the table II.

A camera with a frame rate of 30Hz was used to capture the posture of robotic fish under different swimming motions in a cycle, as shown in Fig. 17. It can be seen that the robotic fish can present corresponding body posture according to different

TABLE II
PARAMETER SETTINGS FOR DIFFERENT MOTIONS IN STATIONARY TESTS

Motion	M	B	R	k
Cruising-straight	3	0	1	π
Cruising-turn	3	1	1	π
C-turn	3	3	3	$\pi/8$
Small radius turn	3	6	3	$\pi/8$
S-turn	3	3	0.5	π

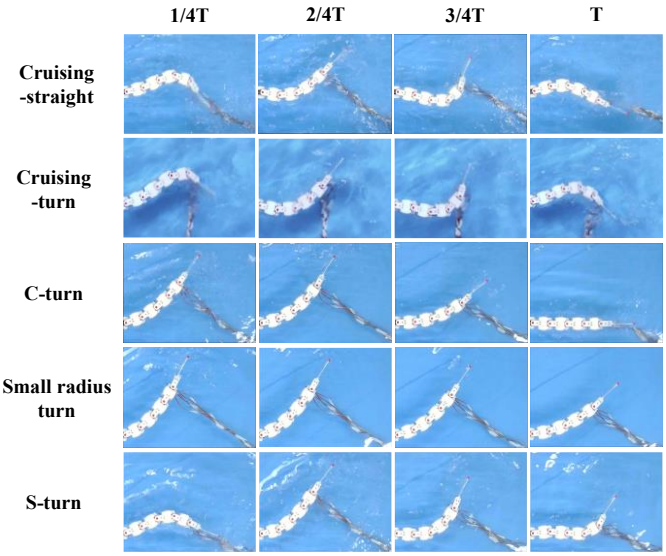

Fig. 17. Snapshot sequence of the robotic fish body posture with different swimming motions

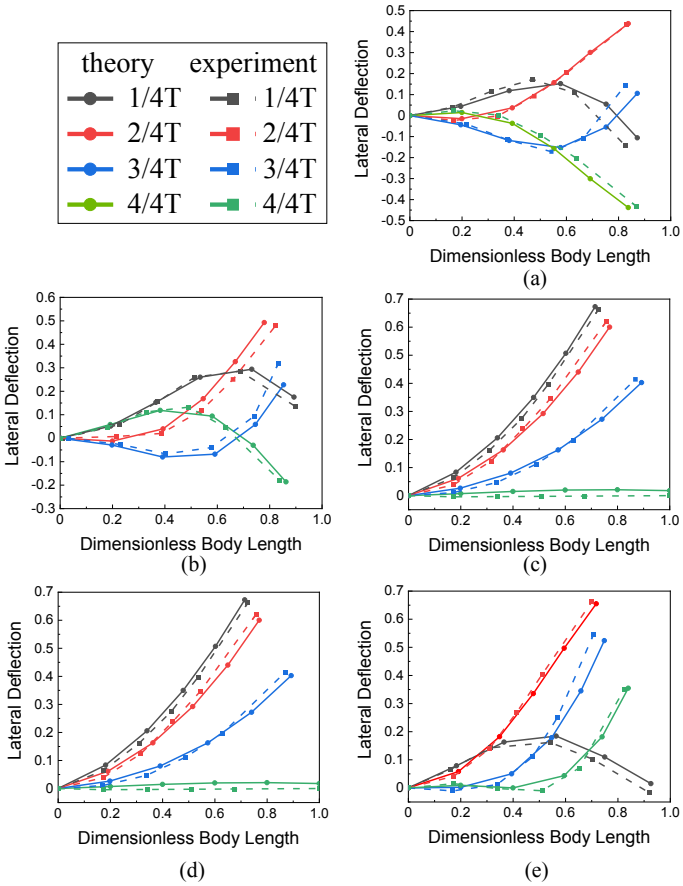

Fig. 18. The comparison of experiment and theory of the robotic fish body midline. (a) Cruising-straight. (b) C-turn. (c) Small radius turn. (d) S-turn.

commands. There are 5 markers pasted on the joints and the end of the robotic fish, respectively. Through the utilization of the GetData software to extract the coordinates of markers at different times, the trajectory of the midline of the robotic fish in experiments can be ascertained. By discretizing the unit length line into 5 segments and applying the same input as the control signal to each connects point, we can obtain the theoretical midline of the robotic fish. Comparing the normalized experimental midline with the theoretical midline, we can find that the errors between the experiment and theory are very small (Fig. 18), which also includes visual angle and assembly errors. It is proved that the method has high accuracy in controlling the robotic fish with different motions.

D. Free swimming tests

Although we can make the robotic fish swing according to the general kinematics model, it is still not clear how it will swim. The experiments in this part will be combined with the simulation results of the dynamics model in Section III to further analyze the swimming performance of different motions described by the general kinematic model.

To ensure the accuracy of the simulation model, set the model parameters according to the actual data of the prototype. The number of links: N = 6; the major radius of links: **a** = diag[0.045, 0.045, 0.045, 0.045, 0.045, 0.045] (m); the minor radius of links: **b** = diag[0.04, 0.04, 0.04, 0.04, 0.04, 0.005] (m); the length of links: **l** = diag[0.115, 0.08, 0.08, 0.08, 0.08, 0.11] (m); the mass of links: **m** = diag[0.2, 0.16, 0.16, 0.16, 0.16, 0.01] (kg). In terms of hydrodynamic parameters, the approximate range can be estimated based on empirical values, but to improve the accuracy of the model, it is still necessary to determine specific parameters in combination with experimental results. After comparing the simulation results and experimental results under different swimming motions, we set the hydrodynamic parameters as: C_f = 0.03 (drag coefficients in tangential direction); C_D = 0.2 (drag coefficients in normal direction); C_M = 1 (the added inertia coefficient). Due to the low swimming speed of robotic fish in this simulation, add mass effects can be ignored [55], so we regard C_A as 0. The water density ρ is set to 1000kg/m^3. For the PD controller that converts the angle to torque, we set K_p and K_d to 100 and 0.1 respectively.

After constructing the simulation environment, we begin to analyze the characteristics of different swimming motions. Multiple motions usually do not appear in the same type of fish. For example, an Anguilliform swimmer with a slender body can make S-turn, while a Carangiform swimmer tends to use C-turn due to the shorter part of the body to swing. To enable the multi-joint robotic fish to imitate different types of swimmers, we made slight adjustments in the structure and control method according to different swimming motions during simulation and experiment. In Cruising-straight, Cruising-turn and S-turn, the Anguilliform swimmer is regarded as an imitation object. Each joint of the robotic fish is driven and equipped with an eel-like tail. In C-turn and Small radius turn, select Carangiform swimmer as the imitation object. Since the bending part of this kind of swimmer is mainly concentrated on the back end of the body, the front joints of the robotic fish will not change during swimming. Only the last two joints will be applied with driving torque to fit the curve, and a tail similar to the Carangiform swimmer will be installed. The shapes of the two tails are shown in Fig. 19. In this test, we set c_0 = 0, c_1= 0.05, c_2 = 0.15, and the frequency of all swimming motions is 1 Hz. The settings of the rest parameters are shown in the table III.

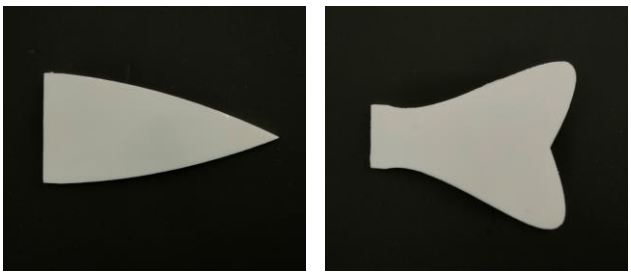

(a) (b)

Fig. 19. Different types of fish tails used in free swimming test. (a) Anguilliform tail. (b) Carangiform tail.

TABLE III
PARAMETER SETTINGS FOR DIFFERENT MOTIONS IN FREE SWIMMING TESTS

Motion	M	B	R	k
Cruising-straight	3	0	1	π
Cruising-turn	3	1	1	π
C-turn	5	5	10	$\pi/8$
Small radius turn	5	6	10	$\pi/8$
S-turn	3	3	0.5	π

We pasted two markers on the head of the robotic fish and test it in a tank with the dimensions of 3.0m × 2.0m × 0.6m. Since our robotic fish does not carry sensors, we need to rely on external equipment to obtain its position information. A camera with a frame rate of 30Hz was installed on top of the tank, 1.5m above the water. The experimental platform is shown in Fig. 20.

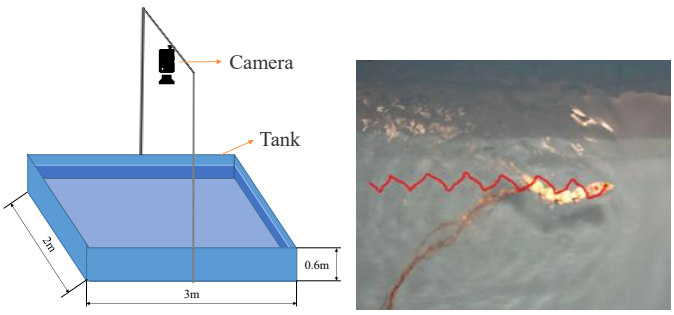

(a) (b)

Fig. 20. The experimental platform. (a) The layout of experimental equipment. (b) The images captured by the camera.

After recording the free swimming of the robotic fish, we used Kinovea software to analyze the video to get the coordinates of the markers. This allows us to obtain the change in position and attitude of the robotic fish under different motions. Fig. 21 (a) exhibits the robotic fish's position and linear velocity during Cruising-straight. The robotic fish swims forward in a reciprocating yaw. Due to the influence of the cable, the experimental linear velocity gradually decreases over time, but remains near the simulated value. Fig. 21 (b) - (e) represent the robotic fish's position and angular velocity in Cruising-turn, S-turn, C-turn, and Small radius turn respectively. It shows that all these motions have successfully realized the turning of the robotic fish. The Cruising-turn has minimum angular velocity and the largest turning radius. The body posture of the S-turn is similar to the Cruising-turn, but due to its characteristics of bending quickly and restoring slowly, its turning performance is better than Cruising-turn. In the same M (amplitude state) and the same R (time ratio), the turning radius and angular velocity of the Small radius turn are smaller than C-turn, which is consistent with its characteristics. Comparing the simulation and experimental results of each swimming motion, we can see that the trends are similar, which verified the accuracy of the dynamic model. Keeping the parameter settings in Table III constant and varying the frequency of each motion in the free swimming test, the trend in velocity with frequency can be observed, as shown in table IV. Based on the velocity of Cruising-straight at different frequencies, we calculated the Strouhal numbers of the robotic fish, with values ranging from 0.76 to 1.13.

Combining the dynamic model of robotic fish with the general kinematic model, it is very convenient to conduct quantitative analysis on different swimming motions of fish. Taking small radius turn as an example. We set $c_0 = 0$, $c_1 = 0.05$, $c_2 = 0.15$, $\omega = 2\pi$, $M = 5$, $R = 10$, $k = \pi/8$, and change B from 6 to 10 to analyze the influence of offset on turning performance. It can be seen from Fig. 22 (a) that with the increase of offset B, the turning radius and average angular velocity of the robotic fish are both decreasing. Then keep $B = 6$, and change R from 6 to 10 to analyze the influence of time ratio. Fig. 22 (b) shows that with the increase of time ratio R, the robotic fish's turning radius decreases, and average angular velocity increases. With this conclusion, we can accurately design the turning gait of robotic fish according to the actual needs. Similarly, other types of gait analysis and design can also

TABLE IV
SWIMMING SPEED AT DIFFERENT FREQUENCIES OF EACH MOTION

Motion	Average linear velocity(m/s)			
	1Hz	1.5Hz	2Hz	2.5Hz
Cruising-straight	0.21	0.31	0.42	0.43
Motion	Average angular velocity(deg/s)			
	1Hz	1.5Hz	2Hz	2.5Hz
Cruising-turn	5.5	24.3	34.6	43.5
C-turn	22.5	25.7	29.5	39.1
Small radius turn	16.4	18.8	21.1	25.9
S-turn	32.7	39.5	44.7	59.3

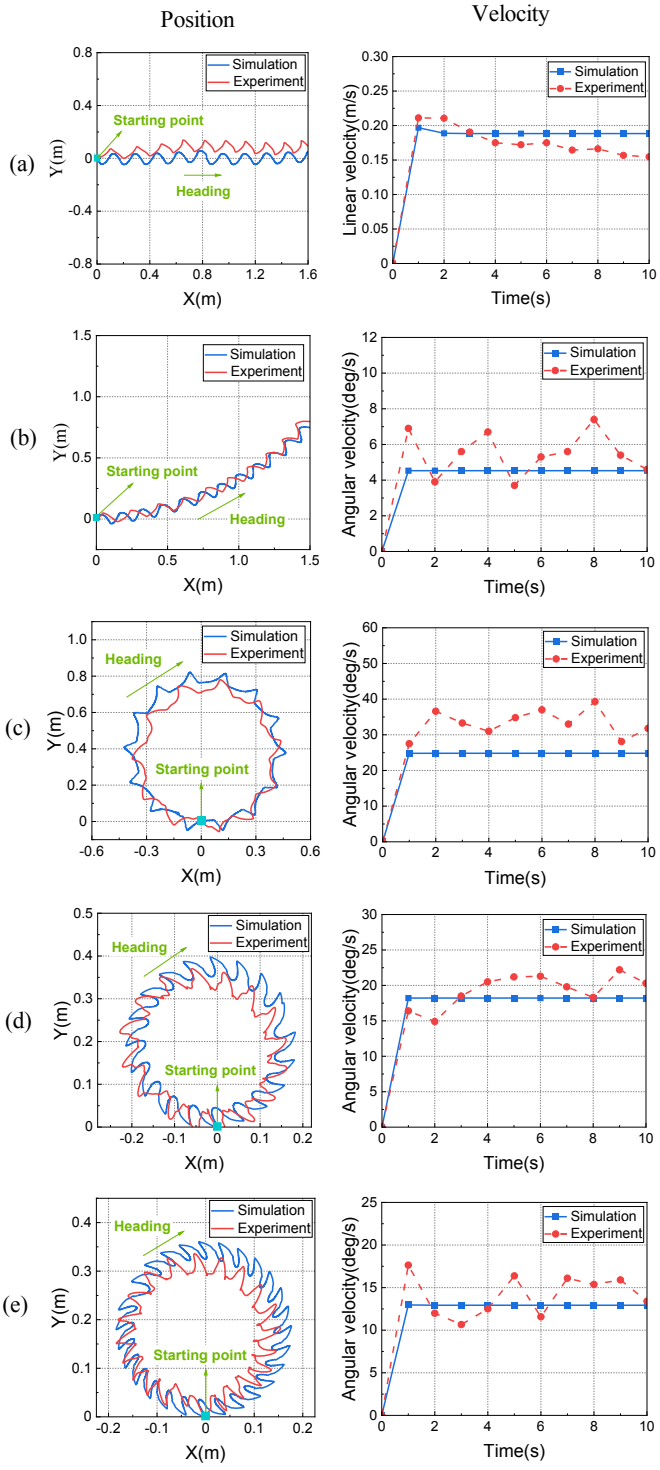

Fig. 21. Various swimming motions performance. (a) Cruising-straight. (b) Cruising-turn. (c) S-turn. (d) C-turn (e) Small radius turn.

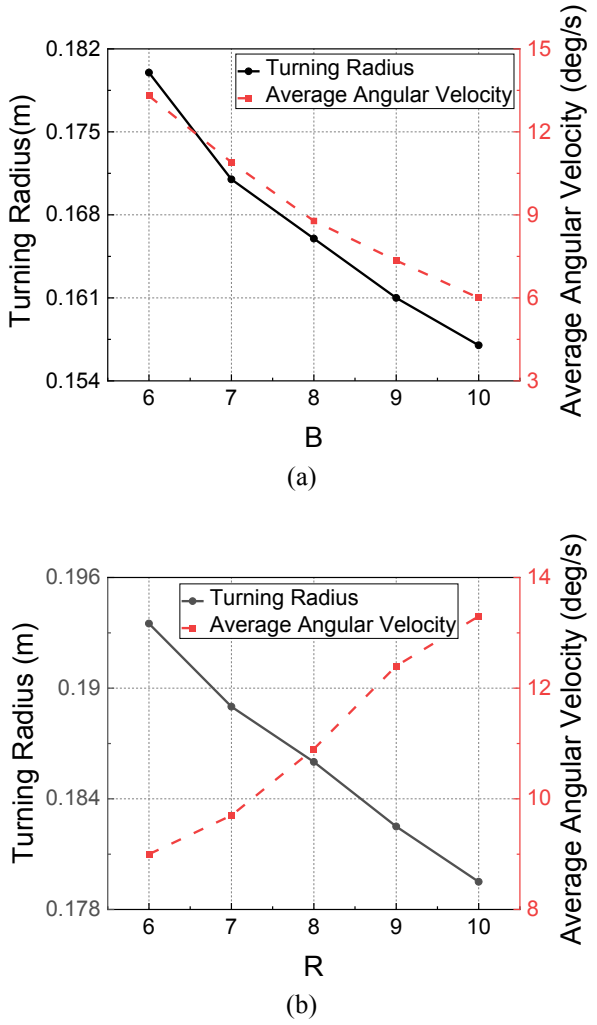

Fig. 22. Quantitative analysis of small radius turn. (a) Effect of B(offset). (b) Effect of R(time ratio).

be realized by this method. Compared with CFD and other numerical simulation methods that require a long calculation period, it is more efficient to study the swimming performance of different gaits through the simulation of dynamic model, which is more suitable for assisting the design of the control algorithm.

V. Conclusion and Discussion

In this paper, we present a general kinematic model which can describe multiple swimming motions of fish such as Cruising-straight, Cruising-turn, C-turn, small radius turn, and S-turn. The model is synthesized by a nonlinear oscillator and a traveling wave equation. By adjusting the M (amplitude), B (offset), R (time ratio), and k (body wavelength) of the model, its form can be switched between the aforementioned swimming motions: when $B = 0$, $R = 1$, and $k > 0$, Cruising-straigth; when $0 < |B| < |M|$, $R = 1$, and $k > 0$, Cruising-turn; when $|B| = |M|$, $R > 1$, and $0 < k \leq \pi/2$, C-turn; when $|B| > |M|$, $R > 1$, and $0 < k \leq \pi/2$, small radius turn; when $|B| \geq |M|$, $R < 1$, and $\pi/2 < k \leq \pi$, S-turn. This facilitates the quantitative analysis of fish's various motions and reduces the difficulty of precise control of multiple gaits of the robotic fish. We also built a multi-joint robotic fish dynamic model and carried out simulation analysis on it based on the general kinematic model. Combined with the experimental results, we validate the feasibility of the general kinematic model guiding the designer to complete the multi-motion control of the robotic fish, and also verified the accuracy of the dynamic model. In addition, the numerical simulation of the robotic fish gait switching process is carried out, which shows the potential of the general kinematic model in the field of numerical simulation. The main contributions can be summarized as follows:

1) The proposed general kinematic model can easily model different swimming motions of fish, which not only greatly benefits the multi-motions control of robotic fishes for roboticists, but also help fish biologists and CFD specialists to study the inherent principles of multiple fish swimming motions. One can simply change the key parameters of the model to generate the interested motions for further study.
2) The systematical method presented in this paper has contained the general kinematic model, dynamic model, and corresponding control method, which can offer the instructional framework for one to develop bioinspired underwater robots.

In the future, we will not rigidly adhere to the existing motion of the real fish, but try to change the parameters in the general kinematics model to get a more interesting gait, and explore more possibilities for robotic fish design. Meanwhile, we will combine machine learning to optimize the parameters in the general kinematic model for different purposes and get the optimal parameter combination of different motions. In addition to its relevance in the field of robotic fish, the general kinematics model can mimic the gait of creatures such as snakes by adjusting the parameters, which is helpful to the study of other rhythmic bionic robots. This is also the potential value that we will continue to explore.

Although the general kinematics model can illustrate various motions of underwater organisms, it still has some limitations. Because it is coupled with the traveling wave equation, the independent variable x in the model corresponds to a unique solution. This makes it difficult to describe large curvature motions, such as a C-turn that bends more than a semicircle, which means that it is hard to cover some fast turns with extremely high turning angles. In the follow-up study, we will try to add more forms of parabolic equations as components to the model to solve this problem.

References

[1] M. Sfakiotakis, D. M. Lane, and J. B. C. Davies, "Review of fish swimming modes for aquatic locomotion," *IEEE Journal of Oceanic Engineering,* vol. 24, no. 2, pp. 237-252, Apr 1999.
[2] J. J. Videler, *Fish swimming*. Springer Science & Business Media, 1993.
[3] H. Hu, "Biologically Inspired Design of Autonomous Robotic Fish at Essex," in *IEEE SMC UK-RI Chapter Conference on Advances in Cybernetic Systems*, 2006, pp. 1–8.
[4] P. Domenici and R. W. Blake, "The kinematics and performance of fish fast-start swimming," *Journal of Experimental Biology,* vol. 200, no. 8, pp. 1165-1178, Apr 1997.

[5] D. G. Harper and R. W. Blake, "Fast-start performance of rainbow trout Salmo gairdneri and northern pike Esox lucius," *Journal of Experimental Biology,* vol. 150, no. 1, pp. 321-342, 1990.
[6] M. J. Lighthill, "Note on the swimming of slender fish," *Journal of Fluid Mechanics,* vol. 9, no. 2, pp. 305-317, 1960.
[7] S. Kern and P. Koumoutsakos, "Simulations of optimized anguilliform swimming," *Journal of Experimental Biology,* vol. 209, no. 24, pp. 4841-4857, Dec 15 2006.
[8] I. Borazjani and F. Sotiropoulos, "On the role of form and kinematics on the hydrodynamics of self-propelled body/caudal fin swimming," *Journal of Experimental Biology,* vol. 213, no. 1, pp. 89-107, Jan 1 2010.
[9] N. Li, H. Liu, and Y. Su, "Numerical study on the hydrodynamics of thunniform bio-inspired swimming under self-propulsion," *Plos One,* vol. 12, no. 3, Mar 31 2017, Art no. e0174740.
[10] A. P. Maertens, A. Gao, and M. S. Triantafyllou, "Optimal undulatory swimming for a single fish-like body and for a pair of interacting swimmers," *Journal of Fluid Mechanics,* vol. 813, pp. 301-345, Feb 25 2017.
[11] E. D. Tytell and G. V. Lauder, "Hydrodynamics of the escape response in bluegill sunfish, Lepomis macrochirus," *Journal of Experimental Biology,* vol. 211, no. 21, pp. 3359-3369, Nov 1 2008.
[12] U. K. Mueller, J. G. M. van den Boogaart, and J. L. van Leeuwen, "Flow patterns of larval fish: undulatory swimming in the intermediate flow regime," *Journal of Experimental Biology,* vol. 211, no. 2, pp. 196-205, Jan 15 2008.
[13] G. Li, U. K. Mueller, J. L. van Leeuwen, and H. Liu, "Body dynamics and hydrodynamics of swimming fish larvae: a computational study," *Journal of Experimental Biology,* vol. 215, no. 22, pp. 4015-4033, Nov 2012.
[14] M. Gazzola, W. M. Van Rees, and P. Koumoutsakos, "C-start: optimal start of larval fish," *Journal of Fluid Mechanics,* vol. 698, pp. 5-18, May 10 2012.
[15] A. Leroyer and M. Visonneau, "Numerical methods for RANSE simulations of a self-propelled fish-like body," *Journal of Fluids and Structures,* vol. 20, no. 7, pp. 975-991, Oct 2005.
[16] G. Liu, Y.-L. Yu, and B.-G. Tong, "Flow control by means of a traveling curvature wave in fishlike escape responses," *Physical Review E,* vol. 84, no. 5, Nov 18 2011, Art no. 056312.
[17] Y. K. Feng, H. X. Liu, Y. Y. Su, and Y. M. Su, "Numerical study on the hydrodynamics of C-turn maneuvering of a tuna-like fish body under self-propulsion," *Journal of Fluids and Structures,* vol. 94, Apr 2020, Art no. 102954.
[18] M. S. Triantafyllou and G. S. Triantafyllou, "An Efficient Swimming Machine," *Scientific American,* vol. 272, no. 3, pp. 64-70, 1995.
[19] S. B. Behbahani and X. Tan, "Design and Modeling of Flexible Passive Rowing Joint for Robotic Fish Pectoral Fins," *IEEE Transactions on Robotics,* vol. 32, no. 5, pp. 1119-1132, 2016.
[20] B. Chen and H. Jiang, "Body Stiffness Variation of a Tensegrity Robotic Fish Using Antagonistic Stiffness in a Kinematically Singular Configuration," *IEEE Transactions on Robotics,* vol. 37, no. 5, pp. 1712-1727, 2021.
[21] Y. Wang *et al.*, "A biorobotic adhesive disc for underwater hitchhiking inspired by the remora suckerfish," *Science Robotics,* vol. 2, no. 10, p. eaan8072, 2017.
[22] Z. Wu, J. Yu, J. Yuan, and M. Tan, "Towards a Gliding Robotic Dolphin: Design, Modeling, and Experiments," *IEEE-Asme Transactions on Mechatronics,* vol. 24, no. 1, pp. 260-270, Feb 2019.
[23] Q. Zhong *et al.*, "Tunable stiffness enables fast and efficient swimming in fish-like robots," *Science Robotics,* vol. 6, no. 57, p. eabe4088, 2021.
[24] T. Zhang *et al.*, "From Simulation to Reality: A Learning Framework for Fish-Like Robots to Perform Control Tasks," *IEEE Transactions on Robotics,* vol. 38, no. 6, pp. 3861-3878, 2022.
[25] R. Thandiackal *et al.*, "Emergence of robust self-organized undulatory swimming based on local hydrodynamic force sensing," *Science Robotics,* vol. 6, no. 57, p. eabf6354, 2021.
[26] F. Berlinger, M. Gauci, and R. Nagpal, "Implicit coordination for 3D underwater collective behaviors in a fish-inspired robot swarm," *Science Robotics,* vol. 6, no. 50, p. eabd8668, 2021.
[27] C. Armanini, M. Farman, M. Calisti, F. Giorgio-Serchi, C. Stefanini, and F. Renda, "Flagellate underwater robotics at macroscale: design, modeling, and characterization," *IEEE Transactions on Robotics,* vol. 38, no. 2, pp. 731-747, 2021.
[28] D. Romano, G. Benelli, E. Donati, D. Remorini, A. Canale, and C. Stefanini, "Multiple cues produced by a robotic fish modulate aggressive behaviour in Siamese fighting fishes," *Scientific reports,* vol. 7, no. 1, p. 4667, 2017.
[29] A. Jusufi, D. M. Vogt, R. J. Wood, and G. V. Lauder, "Undulatory swimming performance and body stiffness modulation in a soft robotic fish-inspired physical model," *Soft robotics,* vol. 4, no. 3, pp. 202-210, 2017.
[30] Y. Zhong, Z. Li, and R. Du, "A Novel Robot Fish With Wire-Driven Active Body and Compliant Tail," *IEEE-Asme Transactions on Mechatronics,* vol. 22, no. 4, pp. 1633-1643, Aug 2017.
[31] Q. Wang, Z. Hong, and Y. Zhong, "Learn to swim: Online motion control of an underactuated robotic eel based on deep reinforcement learning," *Biomimetic Intelligence and Robotics,* vol. 2, no. 4, p. 100066, 2022/12/01/ 2022.
[32] Y. Zhong, Y. Chen, C. Wang, Q. Wang, and J. Yang, "Research on Target Tracking for Robotic Fish Based on Low-Cost Scarce Sensing Information Fusion," *IEEE Robotics and Automation Letters,* vol. 7, no. 3, pp. 6044-6051, 2022.
[33] Y. Zhong, J. Song, H. Yu, and R. Du, "Toward a Transform Method From Lighthill Fish Swimming Model to Biomimetic Robot Fish," *IEEE Robotics and Automation Letters,* vol. 3, no. 3, pp. 2632-2639, Jul 2018.
[34] J. Yu, M. Wang, H. Dong, Y. Zhang, and Z. Wu, "Motion Control and Motion Coordination of Bionic Robotic Fish: A Review," *Journal of Bionic Engineering,* vol. 15, no. 4, pp. 579-598, Jul 2018.
[35] Z. Su, J. Yu, M. Tan, and J. Zhang, "Implementing Flexible and Fast Turning Maneuvers of a Multijoint Robotic Fish," *IEEE-Asme Transactions on Mechatronics,* vol. 19, no. 1, pp. 329-338, Feb 2014.
[36] J. Yu, L. Liu, L. Wang, M. Tan, and D. Xu, "Turning control of a multilink biomimetic robotic fish," *IEEE Transactions on Robotics,* vol. 24, no. 1, pp. 201-206, Feb 2008.
[37] J. Z. Yu, M. Tan, S. Wang, and E. Chen, "Development of a biomimetic robotic fish and its control algorithm," *IEEE Transactions on Systems Man and Cybernetics Part B-Cybernetics,* vol. 34, no. 4, pp. 1798-1810, Aug 2004.
[38] J. Liu and H. Hu, "Biological Inspiration: From Carangiform Fish to Multi-Joint Robotic Fish," *Journal of Bionic Engineering,* vol. 7, no. 1, pp. 35-48, Mar 2010.
[39] C. Rossi, J. Colorado, W. Coral, and A. Barrientos, "Bending continuous structures with SMAs: a novel robotic fish design," *Bioinspiration & biomimetics,* vol. 6, no. 4, p. 045005, 2011.
[40] A. J. Ijspeert, A. Crespi, D. Ryczko, and J.-M. Cabelguen, "From swimming to walking with a salamander robot driven by a spinal cord model," *Science,* vol. 315, no. 5817, pp. 1416-1420, Mar 9 2007.
[41] F. Xie, Y. Zhong, R. Du, and Z. Li, "Central Pattern Generator (CPG) Control of a Biomimetic Robot Fish for Multimodal Swimming," *Journal of Bionic Engineering,* vol. 16, no. 2, pp. 222-234, Mar 2019.
[42] J. Yu, R. Ding, Q. Yang, M. Tan, W. Wang, and J. Zhang, "On a Bio-inspired Amphibious Robot Capable of Multimodal Motion," *IEEE-Asme Transactions on Mechatronics,* vol. 17, no. 5, pp. 847-856, Oct 2012.
[43] A. J. Ijspeert, "Central pattern generators for locomotion control in animals and robots: A review," *Neural Networks,* vol. 21, no. 4, pp. 642-653, May 2008.
[44] J. Yu, M. Tan, J. Chen, and J. Zhang, "A Survey on CPG-Inspired Control Models and System Implementation," *IEEE Transactions on Neural Networks and Learning Systems,* vol. 25, no. 3, pp. 441-456, Mar 2014.
[45] P. V. Y. Alvarado and K. Youcef-Toumi, "Design of machines with compliant bodies for biomimetic locomotion in liquid environments," *Journal of Dynamic Systems Measurement and Control-Transactions of the Asme,* vol. 128, no. 1, pp. 3-13, Mar 2006.
[46] R. Du, Z. Li, K. Youcef-Toumi, and P. V. y Alvarado, *Robot fish: Bio-inspired fishlike underwater robots*. Springer, 2015.
[47] M. Sato, M. Fukaya, and T. Iwasaki, "Serpentine locomotion with robotic snakes," *IEEE Control Systems Magazine,* vol. 22, no. 1, pp. 64-81, 2002.
[48] F. Boyer, M. Porez, and W. Khalil, "Macro-continuous computed torque algorithm for a three-dimensional eel-like robot," *IEEE Transactions on Robotics,* vol. 22, no. 4, pp. 763-775, 2006.
[49] K. A. McIsaac and J. P. Ostrowski, "Motion planning for anguilliform locomotion," *IEEE Transactions on Robotics and Automation,* vol. 19, no. 4, pp. 637-652, 2003.
[50] E. Kelasidi, K. Y. Pettersen, J. T. Gravdahl, and P. Liljebäck, "Modeling of underwater snake robots," in *2014 IEEE International Conference on Robotics and Automation (ICRA)*, 2014: IEEE, pp. 4540-4547.
[51] E. Kelasidi, P. Liljebäck, K. Y. Pettersen, and J. T. Gravdahl, "Integral Line-of-Sight Guidance for Path Following Control of Underwater Snake Robots: Theory and Experiments," *IEEE Transactions on Robotics,* vol. 33, no. 3, pp. 610-628, 2017.
[52] Z. Hong, Q. Wang, and Y. Zhong, "Parameters Optimization of Body Wave Control Method for Multi-joint Robotic Fish Based on Deep

Reinforcement Learning," in *2022 IEEE International Conference on Robotics and Biomimetics (ROBIO)*, 2022, pp. 604-609.
[53] Y. Li, J. Song, L. Yin, B. Jin, B. Yin, and Y. Zhong, "Hydrodynamics and Musculature Actuation of Fish during a Fast Start," *Applied Sciences,* vol. 13, no. 4, p. 2365, 2023.
[54] Y. Zhong, J. Wu, C. Wang, Y. Li, and J. Song, "Hydrodynamic effects of the caudal fin shape of fish in carangiform undulatory swimming," *Proceedings of the Institution of Mechanical Engineers, Part C: Journal of Mechanical Engineering Science,* vol. 236, no. 12, pp. 6385-6394, 2022.
[55] T. Fossen, *Handbook of Marine Craft Hydrodynamics and Motion Control*. John Wiley & Sons, 2011.

Yong Zhong (Member, IEEE) received the B.Eng. degree in mechanical design, manufacturing and automation from the Huazhong University of Science and Technology, Hubei, China, in 2011, and the M.Eng. degree in control engineering from the University of Chinese Academy of Sciences, Beijing, China, in 2014, and the Ph.D. degree in Mechanical and Automation Engineering from the Chinese University of Hong Kong, Shatin, Hong Kong, in 2017. He was a research fellow at National University of Singapore from 2017 to 2019.

He is currently an Associate Professor with Shien-Ming Wu School of Intelligent Engineering, South China University of Technology. His research interests include bioinspired robots, soft robots, intelligent diagnosis and control.

Zicun Hong (Graduate Student Member, IEEE) received the B.E. degree in process equipment and control engineering from China University of Petroleum, Qingdao, China, in 2018, and the M.E. degree in power engineering from China University of Petroleum, Beijing, China, in 2021.

He is currently working toward the Ph.D. degree in mechanical engineering at South China University of Technology, Guangzhou, China. His research interests include bioinspired underwater robots and intelligent control systems.

Yuhan Li received the B.E. degree in energy and power engineering in 2020 and the M.E degree in mechanical engineering in 2023 from South China University of Technology, Guangzhou, China.

His research interests include computational fluid dynamics.

Junzhi Yu (Fellow, IEEE) received the B.E. degree in safety engineering and the M.E. degree in precision instruments and mechanology from the North University of China, Taiyuan, China, in 1998 and 2001, respectively, and the Ph.D. degree in control theory and control engineering from the Institute of Automation, Chinese Academy of Sciences, Beijing, China, in 2003.

From 2004 to 2006, he was a Postdoctoral Research Fellow with the Center for Systems and Control, Peking University, Beijing. In 2006, he was an Associate Professor with the Institute of Automation, Chinese Academy of Sciences, where he was a Full Professor in 2012. In 2018, he joined the College of Engineering, Peking University, as a Tenured Full Professor. His current research interests include intelligent robots, motion control, and intelligent mechatronic systems.